

Non-isothermal crystallization kinetics and melting behavior of EAA with different acrylic acid content

Jun Zhang · Shuangjun Chen · Jun Su · Xuming Shi ·
Jing Jin · Xiaolin Wang · Zhongzi Xu

Received: 10 October 2008 / Accepted: 12 May 2009 / Published online: 10 June 2009
© Akadémiai Kiadó, Budapest, Hungary 2009

Abstract Non-isothermal crystallization kinetics and subsequent melting behavior for three kinds of ethylene-acrylic acid copolymer (EAA) are investigated via differential scanning calorimetry (DSC). From the Jeziorny method, the crystallization rate of the primary stage is significantly influenced by the competitive mobility of chains. While the crystallization rate in the secondary stage decreases in order of acrylic acid (AA) content in copolymers. Mo's method can also provide a good fitting. Difference between the Jeziorny method and Mo's method analysis is because of a higher effect of non-crystallizable chain ends. The effective activation energy is also determined via Kissinger's method.

Keywords Crystallization activation energy · Differential scanning calorimetry · Ethylene-acrylic acid copolymers · Non-isothermal crystallization kinetics

Introduction

Ethylene-acrylic acid copolymer (EAA) is a hydrophilic and semi-crystallizable polymer which is widely applied in fields of packing, powder coating, adhesive, hot melt glue, water-based solvent, etc [1]. EAA is produced through random copolymerization of ethylene and acrylic acid

(AA) monomers. Introduction of polar carboxyl groups lowers tacticity of main chains, resulting in various crystallization behaviors. With the increase of AA content, EAA is more hydrophilic and more hydrogen bonds are formed [2]. Such special structure makes remarkable discrepancy on inter-molecular interaction and chain's mobility between EAA and conventional polyethylene [3].

It is interesting to investigate the effect of AA content on crystallization behavior of EAA because hydrogen bonding of AA group plays significant role in EAA crystallization. Kang et al. [4] examined the effect of AA content on ethylene copolymer crystallization via Fourier transform infrared spectroscopy (FTIR) and observed that hydrogen bonding of AA acted as cross-linking points which produced a lot of monoclinic crystal instead of orthorhombic crystal and reduced crystallinity. In addition, hydrogen bonding broken at high temperature would be distorted during crystallization. Zhao et al. [5] investigated the relation of amorphous region structure and molecular motion with AA content. It was observed that hydrogen bonding can be formed among carboxyl groups in amorphous region. The number of hydrogen bond would grow with the increase of AA content. More fraction of amorphous region in EAA led to more inter-molecular hydrogen bonding, thus chain segment's mobility decreased. What is more, the motion of ethylene chains in amorphous region was also affected by hydrogen bonding; high temperature would destroy the hydrogen bonding among carboxyl, making chains more flexible in amorphous region. This phenomenon is similar to the observation of Xu [6]. Somrang Supaphol et al. [7] did researches on the influence of hydrogen bonding on non-isothermal crystallization and concluded three important points: (1) the increase of AA content would lower the crystallization rate of EAA; (2) amorphous region content played more important role than

J. Zhang (✉) · S. Chen · J. Su · X. Shi · J. Jin · Z. Xu
College of Materials Science and Engineering, Nanjing
University of Technology, Nanjing 210009, China
e-mail: zhangjun@njut.edu.cn

X. Wang
Department of Chemical Engineering, Tsinghua University,
Beijing 100084, China

molecular weight in crystallization at the same AA content; (3) the lower the AA content, the higher the crystallinity, the thicker the lamella, and the shorter the melt range.

In this study, a method of non-isothermal crystallization which is closely related to manufacture progress is employed to study the effect of AA content on the crystallization kinetics of EAA. Differential scanning calorimetry measurement (DSC) is used to characterize the non-isothermal crystallization of EAA (at three different AA content) which are analyzed and profiled by Jeriorny, Ozawa and Mo's methods. Kissinger method also is used to calculate crystallization activation energy.

Experimental

Materials

Three grades of EAA with various amount of AA content (Dow Chemical Company, USA) are given in Table 1 and used without any further treatment. The AA co-monomer can be considered to be randomly distributed along the copolymer chains.

Differential scanning calorimetry measurements

The non-isothermal crystallization and the subsequent melting of EAA samples with different AA content were carried out with a differential scanning calorimeter instrument (model Pyris 1, PerkinElmer, USA). Samples weighing 8–10 mg were cut off for the DSC tests. Argon purge gas with a flux of 20 mL min⁻¹ was used to prevent thermal degradation of samples during the scanning. In order to remove the volatile impurities and erase the former thermal history, EAA samples were first heated up to 150 °C at a rapid heating rate of 40 °C min⁻¹ and kept at 150 °C for 5 min. Then they were cooled down from 150 °C to 0 °C at the rate of 2.5, 5, 10, 20 °C min⁻¹ to obtain the non-isothermal crystallization curves, respectively. Finally, the subsequent melting was performed after each step of non-isothermal crystallization by heating run from 0 °C to 150 °C at 10 °C min⁻¹.

The crystallinity (X_c) of the samples was calculated with the following expression:

$$X_c = \frac{\Delta H_f}{\Delta H_f^*} \times 100\% \quad (1)$$

where ΔH_f^* is the enthalpy of fusion of the perfect polyethylene (PE) crystal and ΔH_f is the enthalpy of fusion of the EAA samples, respectively. The value of ΔH_f^* for PE is 277.1 J g⁻¹ [8].

Results and discussion

Non-isothermal crystallization behavior

The characteristic data of non-isothermal crystallization exotherm are listed in Table 2. When cooling rate increases, onset crystallization temperature of EAA (T_c^{on}), peak crystallization temperature of EAA (T_c^p), and final crystallization temperature of EAA (T_c^f) shift towards lower temperature. The trend showed that increasing of cooling rate could delay crystallization process [6, 7]. During the non-isothermal crystallization of the three EAA samples, polymeric chains would have less time to be arranged into crystal lattices when cooling rate increased. ΔH_c decreased

Table 2 Data from DSC curves of three EAA samples at various cooling rates

Sample	ϕ (°C min ⁻¹)	T_c^{on} (°C)	T_c^p (°C)	T_c^f (°C)	ΔT_c (°C)	ΔH_c (J g ⁻¹)
EAA 1410	2.5	87.8	85.3	83.2	4.6	52.93
	5	86.1	83.2	80.9	5.2	53.91
	10	84.2	80.7	77.7	6.5	54.89
	20	81.7	78.1	73.6	8.1	55.50
EAA 3002	2.5	90.0	87.4	85.4	4.6	62.22
	5	88.4	85.5	83.1	5.3	63.90
	10	86.5	83.2	79.9	6.6	67.13
	20	84.3	80.7	74.3	10.0	70.50
EAA 3003	2.5	92.3	89.9	87.9	4.4	71.12
	5	90.7	88.0	85.5	5.2	74.44
	10	88.8	85.6	82.1	6.7	75.03
	20	86.7	83.0	78.2	8.5	76.62

T_c^{on} Onset crystallization temperature of EAA; T_c^p Peak crystallization temperature of EAA; T_c^f Final crystallization temperature of EAA; $\Delta T_c = T_c^{on} - T_c^f$; ΔH_c Crystallization enthalpy of EAA

Table 1 Compositions in weight fractions for EAA copolymers

Grade	Ethylene (wt%)	Acrylic acid (wt%)	Density (g cm ⁻³)	Melt flow rate (g 10 min ⁻¹)	Nomenclature
Primacor1410	90.3	9.7	0.938	1.5	EAA1410
Primacor3002	92.0	8.0	0.936	9.8	EAA3002
Primacor3003	93.5	6.5	0.935	7.8	EAA3003

as the cooling rate increased, which can be regarded as the evidence of insufficient crystallization as cooling rate increased.

In Table 2, the values of T_c^n , T_c^p , T_c^f , and ΔH_c decrease with the increase of AA content at a given cooling rate. For example, at a cooling rate of $5\text{ }^\circ\text{C min}^{-1}$, T_c^p of EAA 1410 is $83.2\text{ }^\circ\text{C}$, T_c^p of EAA 3002 is $85.5\text{ }^\circ\text{C}$, and T_c^p of EAA 3003 is $88.0\text{ }^\circ\text{C}$. This trend is analogous to earlier report [7], in which the author explained that the existence of AA is considered to be non-crystallizable and intra-molecular defects. As a result, the increase in the amount of total comonomer defects resulted in the declining of the number and length of the crystallizable ethylene segments.

Non-isothermal crystallization kinetics

The relative crystallinity (X_t) can be determined by calculating the variation in temperature and enthalpy with initial and final temperature of crystallization based on the following relation [9]:

$$X_t = \frac{\int_{T_0}^T (dH_c/dT)dT}{\int_{T_0}^{T_\infty} (dH_c/dT)dT} \times 100\% \tag{2}$$

where T_0 is the initial temperature of crystallization, T_∞ is the end temperature of crystallization, dH_c is the variation of enthalpy, and dT is the change of temperature.

The relative crystallinity (X_t) as a function of crystallization temperature for EAA at various cooling rates are plotted in Fig. 1. It is apparent that all curves in Fig. 1 show reverse sigmoidal shape, indicating crystal nucleation occurs from the melt and slows down during nucleation growth [10]. After transforming horizontal temperature axis into crystallization time scale, Fig. 2 is plotted. According to Fig. 2, it is found that the higher the cooling rate, the shorter the time of crystallization completion which is similar with previous non-isothermal crystallization studies [11].

(1) Jeziorny method

The classical isothermal crystallization behavior can be described by the classical Avrami equation [12–14]. Based on the assumption that the crystallization temperature is constant, the function is:

$$\log[-\ln(1 - X_t)] = \log Z_t + n \log t \tag{3}$$

where X_t represents the relative crystallinity, n is the Avrami exponent, t stands for the crystallization time and Z_t refers to the growth-rate constant of crystallization. Considering the influence from cooling rate during the practical non-isothermal crystallization, Z_t should not be appropriate for further kinetic evaluation. Jeziorny [9] modified Z_t in Eq. 3 and obtained the following relationship:

$$\log Z_c = \log Z_t / \phi \tag{4}$$

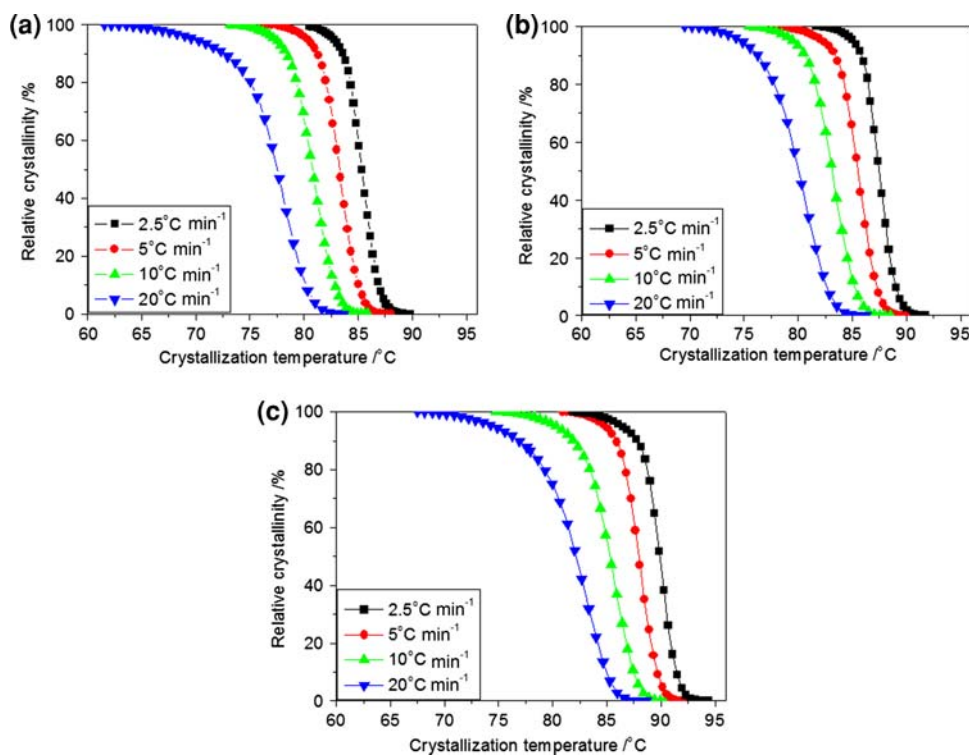


Fig. 1 Plots of relative crystallinity versus crystallization temperature for three EAA samples during the non-isothermal crystallization process. a EAA 1410 (AA = 9.7 wt%), b EAA 3002 (AA = 8.0 wt%), and c EAA 3003 (AA = 6.5 wt%)

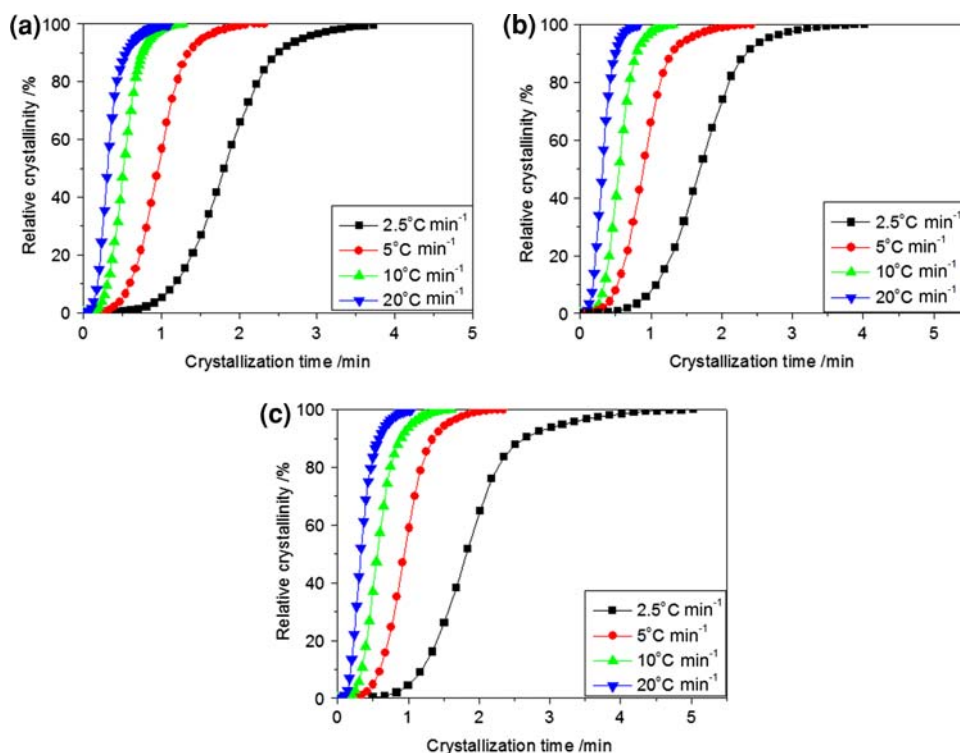


Fig. 2 Plots of relative crystallinity versus crystallization time for three EAA samples during the non-isothermal crystallization process. **a** EAA 1410 (AA = 9.7 wt%), **b** EAA 3002 (AA = 8.0 wt%), and **c** EAA 3003 (AA = 6.5 wt%)

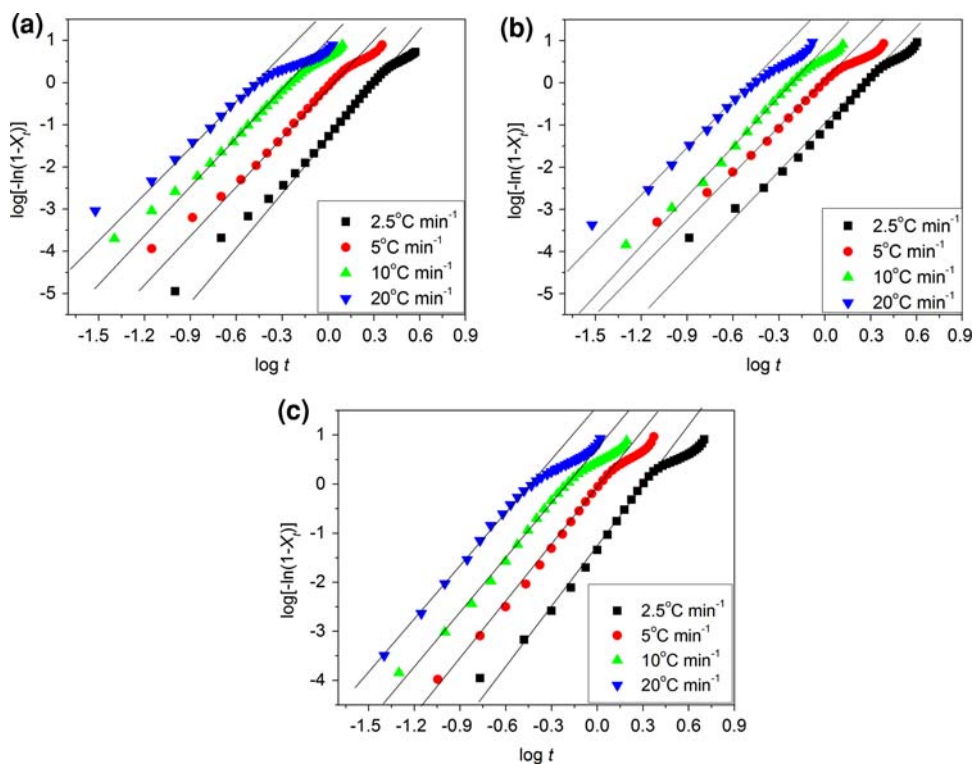


Fig. 3 Plots of $\log[-\ln(1 - X_t)]$ versus $\log t$ for three EAA samples during the non-isothermal crystallization process. **a** EAA 1410 (AA = 9.7 wt%), **b** EAA 3002 (AA = 8.0 wt%), and **c** EAA 3003 (AA = 6.5 wt%)

Table 3 Non-isothermal crystallization kinetic parameters from Jeziorny equation

Sample	ϕ ($^{\circ}\text{C min}^{-1}$)	Kinetic parameters				
		Z_{c1}	n_1	Z_{c2}	n_2	$t_{1/2}$ (min)
EAA 1410	2.5	0.34	3.52	0.59	0.88	1.89
	5	0.84	3.93	0.96	0.97	1.07
	10	1.16	3.82	1.01	0.99	0.58
	20	1.22	4.44	1.03	1.15	0.35
EAA 3002	2.5	0.38	3.85	0.70	1.01	1.70
	5	0.91	3.32	0.94	0.86	0.89
	10	1.19	3.72	1.04	0.93	0.54
EAA 3003	2.5	0.31	3.70	0.74	0.93	1.83
	5	0.90	3.66	0.98	0.98	0.94
	10	1.18	2.83	1.07	1.10	0.57
	20	1.18	3.31	1.08	1.39	0.33

Z_c herein corresponds to the practical rate constant under a non-isothermal condition. ϕ stands for the cooling rate. In Fig. 3, $\log[-\ln(1 - X_t)]$ versus $\log t$ for three EAA samples during the non-isothermal crystallization process at various cooling rates is plotted, respectively. All curves are divided into two stages: the primary crystallization stage and the secondary crystallization stage. The linear part of each curve is almost parallel, indicating analogous mechanism of crystal nucleation and nucleation growth among different EAA.

Kinetic data from the Jeziorny method are listed in Table 3. The value of half crystallization time ($t_{1/2}$) representing the time needed to reach 50% of entire crystallization process is calculated from the DSC curves. It is clear that Z_{c1} increases with the rise of cooling rate, indicating that crystallization rate was enhanced by the increase of cooling rate. At a given cooling rate, the $t_{1/2}$ is the highest for EAA1410 and lowest for EAA3002, indicating EAA3002 is the fastest to crystallize; while EAA1410 is the slowest. This trend can be explained by combining two competing factors of AA content and melt flow rate (MFR) value [7]. It is known that high MFR value reflects that polymeric chains have excellent mobility at melt, and can easier arrange into crystal lattices during crystallization [15]. In addition, AA groups with intramolecular defects would prevent crystallization. AA content of EAA samples follow the order: EAA1410 > EAA3002 > EAA3003; while MFR of EAA samples follow the order: EAA3002 > EAA3003 > EAA1410. The interaction of intra-molecular defects and chains mobility are both contributed to the order of half crystallization time. Obviously, the order of Z_{c1} is identical with that of $t_{1/2}$, showing this model is able to describe the primary stage

of crystallizing process. However, the value of Z_{c2} is the highest for EAA3003 and slowest for EAA1410, indicating that EAA3003 crystallized fastest at the secondary stage while EAA1410 did the lowest. This could be explained by the effect of hydrogen bonding which have not formed at the primary stage of crystallization when temperature is high, but is formed at the secondary stage when temperature is lower [16–19]. Moreover, it is known that hydrogen bonding would prevent crystallizing. Therefore, the higher the AA content, the lower ethylene chain segments for EAA to crystallize; and that is why EAA1410 which possesses the highest AA content crystallizes slowest at the secondary stage of crystallization.

The values of n_1 varied between 3 and 4, indicating uniform nucleation and three dimension nucleation growth. It is obviously that cooling rate has no effect on the mechanism of crystal nucleation and nucleation growth. The value of slope at the second stage is lower than that of the primary stage, indicating the secondary crystallization takes place during the process of crystallization [20]. It verifies that the crystals may grow as small lamellae with lower melting temperature during the secondary crystallization. And the range of n_2 is 1.01–1.68 for three samples indicating the spherulites’ growth transformed into a mixture mode of one-dimensional and two-dimensional space extension due to the spherulites’ impingement and crowding.

(2) Ozawa method

Ozawa also modified the Avrami equation into the following relation by dividing the whole crystallization into countless micro isothermal parts [21]:

$$1 - X(T) = \exp[-K(T)/\phi^m] \tag{5}$$

$$\log[-\ln(1 - X(T))] = \log K(T) - m \log \phi \tag{6}$$

where $X(T)$ is relative crystallinity integrated by temperature, ϕ is cooling rate, $K(T)$ is function of T , and m is index of Ozawa.

Data point folded lines in Fig. 4 indicated the failure of Ozawa’s model. AA units introduced in main chains led to apparent secondary crystallization of EAA, which is lack of sufficient consideration in Ozawa’s model. As is shown in Table 2, the cooling rate influenced the crystallization behavior apparently. The final temperature referring to the secondary crystallization of the exotherm in trace ($\phi = 2.5 \text{ }^{\circ}\text{C min}^{-1}$) just accorded with the beginning of crystallization in trace of $\phi = 20 \text{ }^{\circ}\text{C min}^{-1}$. Thus, the deviation from the Ozawa equation for the non-isothermal crystallization of EAA may be due to the crystallization under the different cooling rates at a given temperature. Such deviation was also been reported in other non-isothermal crystallization studies [22, 23].

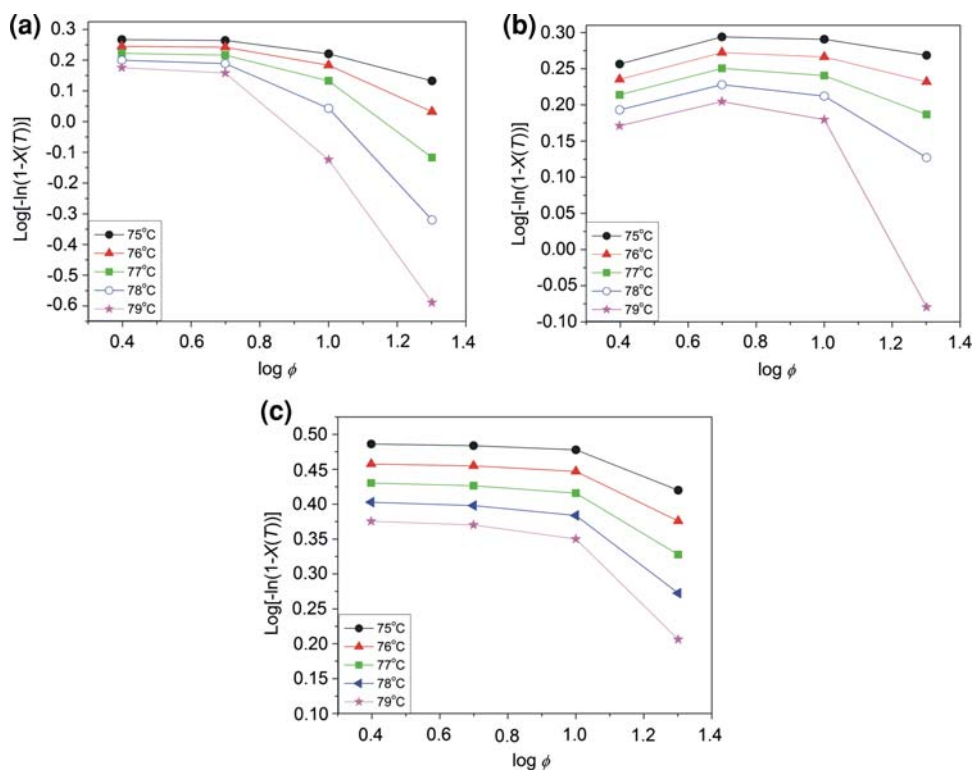


Fig. 4 Plots of $\log[-\ln(1 - X(T))]$ versus $\log \phi$ for three EAA samples during the non-isothermal crystallization process. **a** EAA 1410 (AA = 9.7 wt%), **b** EAA 3002 (AA = 8.0 wt%), and **c** EAA 3003 (AA = 6.5 wt%)

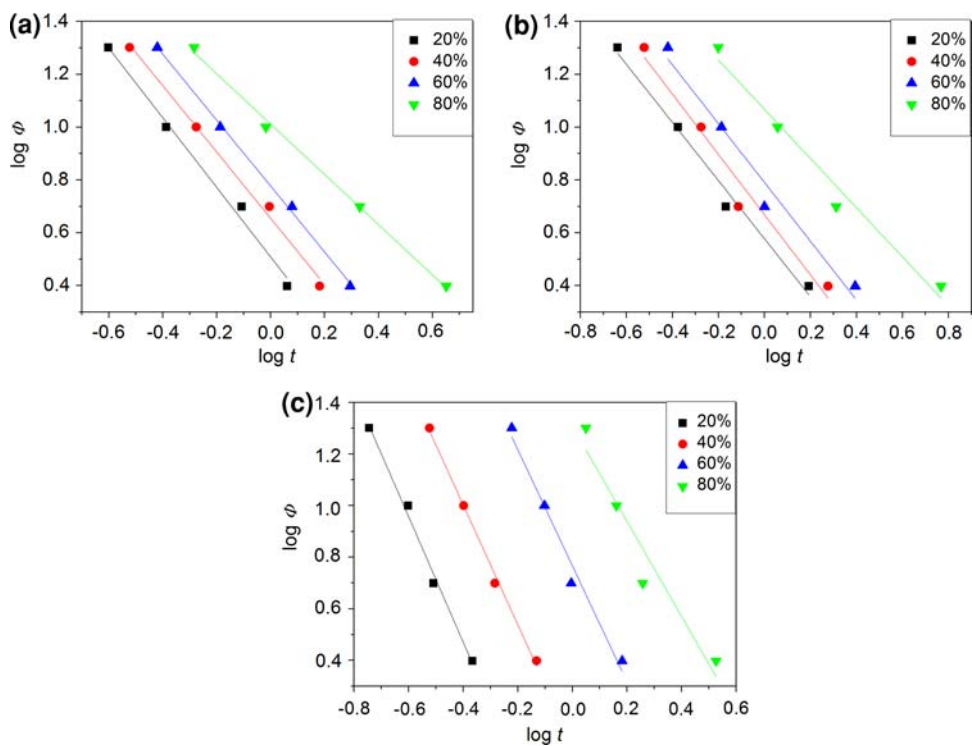


Fig. 5 Plots of $\log \phi$ versus $\log t$ for three EAA samples during the non-isothermal crystallization process. **a** EAA 1410 (AA = 9.7 wt%), **b** EAA 3002 (AA = 8.0 wt%), and **c** EAA 3003 (AA = 6.5 wt%)

Table 4 Non-isothermal crystallization kinetic parameters from Mo's method

Sample	X_t (%)	20	40	60	80
EAA 1410	$F(T)$	3.88	5.16	6.58	10.79
	a	1.32	1.26	1.25	0.95
EAA 3002	$F(T)$	4.15	5.30	6.73	11.01
	a	1.10	1.14	1.11	0.93
EAA 3003	$F(T)$	3.61	4.61	5.72	8.67
	a	2.44	2.32	2.25	1.85

(3) Mo's method

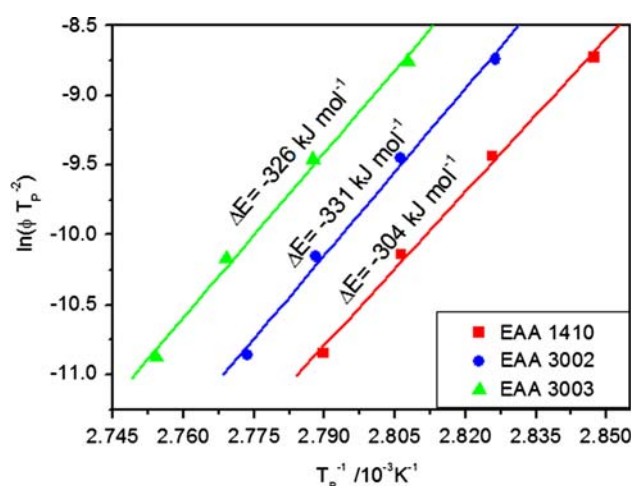
In order to use a method to describe exactly the non-isothermal crystallization process, Mo et al. [18, 24–27] suggested a significant and practical kinetic approach by combining the Avrami equation with the Ozawa equation to conclude the following equations:

$$\log Z_t + n \log t = \log K(T) - m \log \phi. \quad (7)$$

Assuming that $F(T) = [K(T)/Z_t]^{1/m}$ and $a = n/m$, the parameter $F(T)$ has a definite physical and practical meaning and is the value of cooling rate which has to be chosen at a unit crystallization time when the measured system amounts to a certain degree of crystallinity, the parameter a is the ratio of the Avrami exponent, n , to the Ozawa exponent, m . The final form was obtained:

$$\log \phi = \log F(T) - a \log t. \quad (8)$$

At the given relative crystallinity (20, 40, 60, and 80%) of the three grades of EAA copolymers, the plots of $\log \phi$ versus $\log t$ are illustrated in Fig. 5. All these plots exhibit a good linear relation. The values of a and $F(T)$, summarized in Table 4 were calculated from the slope and the intercept of plots. As mentioned above, given the same relative crystallinity, $F(T)$ declines as the crystallization rate increases. From Table 4, it is noted that $F(T)$ for all EAA copolymers increases with the increase of relative degree of crystallinity, which means, in order to reach higher relative crystallinity within a given time, stronger cooling condition is needed. Besides, the crystallization rate of the three grades of EAA is as the following order: EAA3003 > EAA1410 > EAA3002. EAA3003 has the highest crystallization rate indicating that this resin (having the lowest amount of total co-monomer defects) should have the highest tendency to crystallize, which is contrary to others with higher amount of total co-monomer defects. However, an interesting scenario can be observed on EAA3002 and EAA1410 copolymers, since EAA3002 has the fewer amounts of non-crystallizable co-monomers which induce higher crystallization ability, while the results from Mo's method disobey this suppose. Two competition effects occur in this situation: first, the high MFR value means low molecular weight which makes a


Fig. 6 Plots of $\ln(\phi/T_p^2)$ versus $1/T_p$ for three EAA samples

high amount of non-crystallizable chain ends. On the other hand, a low molecular weight also means high mobility. EAA1410 crystallizes more readily, due to the higher amount of non-crystallizable chain ends which affect the crystallization of the polymer more predominantly than the higher mobility [7].

Crystallization activation energy

There are many reports on calculation of crystallization activation energy [28], such as Peggy [29], Augis [30], and Kissinger [31–33]. In this study, Kissinger method is utilized in the following equation:

$$\frac{d[\ln(\phi/T_p^2)]}{d(1/T_p)} = \frac{-\Delta E_C}{R} \quad (9)$$

where T_p is the peak crystallization temperature, ϕ is the cooling rate, R is the universal gas constant, and ΔE_c is the activation energy of crystallization.

The activation energy ΔE calculated by Eq. 9 was plotted in Fig. 6. The effective energy barrier for non-isothermal crystallization can be estimated from the slope of the plot. The ΔE values of all samples follow the order: EAA3002 < EAA3003 < EAA1410, suggesting that EAA3002 is the easiest to crystallize, while EAA1410 is the most difficult one to do so. For EAA3003 and EAA3002, the two competition factors AA content and chain mobility are both responsible for this result which is similar to results from Jeziorny, Ozawa, and Mo's method equation.

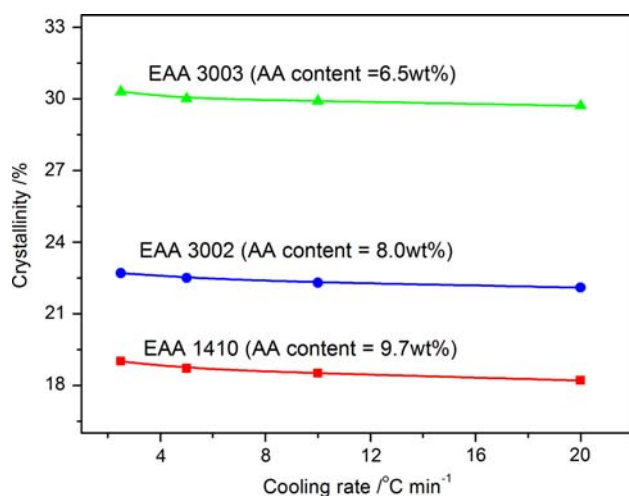
Melting behavior

Table 5 summarizes subsequent endothermic data of EAA after non-isothermal crystallization at various cooling rates. All samples are heated at $10 \text{ }^\circ\text{C min}^{-1}$ heating rate. EAA begins to melt from a comparatively lower temperature.

Table 5 Subsequent melting DSC results of three EAA samples after non-isothermal crystallization

Sample	ϕ ($^{\circ}\text{C min}^{-1}$)	T_m^{on} ($^{\circ}\text{C}$)	T_m^p ($^{\circ}\text{C}$)	T_m^f ($^{\circ}\text{C}$)	ΔT_m ($^{\circ}\text{C}$)	ΔH_m (J g^{-1})	X_c (%)
EAA 1410	2.5	87.7	98.3	102.8	15.1	52.68	19.0
	5	86.7	97.9	103.4	16.7	51.94	18.7
	10	85.6	98.8	103.1	17.5	51.33	18.5
	20	85.0	98.3	103.0	18.0	50.57	18.2
EAA 3002	2.5	91.6	100.3	104.4	12.8	63.00	22.7
	5	90.8	99.9	104.8	14.0	62.40	22.5
	10	90.0	99.6	104.6	14.6	61.87	22.3
	20	89.2	99.4	104.6	15.4	61.16	22.1
EAA 3003	2.5	94.5	103.0	106.7	12.2	84.03	30.3
	5	94.1	102.6	106.7	12.6	83.06	30.0
	10	93.5	102.8	106.7	13.2	82.87	29.9
	20	92.9	102.1	106.7	13.8	82.37	29.7

T_m^{on} Onset melting temperature of EAA, T_m^p Peak melting temperature of EAA, T_m^f Final melting temperature of EAA, $\Delta T_m = T_m^f - T_m^{on}$, ΔH_m Melting enthalpy of EAA, X_c Crystallinity of EAA

**Fig. 7** Plots of cooling rate versus crystallinity for three EAA samples

EAA 1410 whose AA content is the highest among the others possesses the widest range of melting temperature. T_m^{on} , T_m^p , and T_m^f are slightly affected by changes of cooling rate. The melting enthalpy (ΔH_m) also slightly decreases as the cooling rate rises, indicating time is not enough for all chains to be arranged into crystal lattices. From Jeziorny and Mo's methods, EAA3003 crystallizes fastest at the beginning of crystallization and has the highest crystallinity and T_m^p . According to results of crystallization activation energy, the crystallization of EAA has transformed from nucleation controlled model at the beginning to overall growth model gradually.

Figure 7 compares the crystallinity of three EAA at different cooling rates. Comparing with influences from cooling rate, the AA content in EAA affects the crystallinity of polymer decisively. AA units are introduced into

the backbone of copolymer, which act as intervals of crystallizable ethylene chain segments. The crystallization is hindered as the chain regularity is disturbed randomly. Higher co-monomer content in copolymer leads to lower crystallinity [34].

Conclusions

In this research, the non-isothermal crystallization kinetics of three kinds of EAA samples with different AA content was evaluated by DSC via the Jeziorny method, Ozawa method, and Mo's method. Both the Jeziorny and Mo's method could profile the non-isothermal crystallization behavior appropriately, while Ozawa model was not suitable. Results from the Jeziorny method showed that at the primary crystallization stage, the crystallization rate decreased in the following order: EAA3002 > EAA3003 > EAA1410, which was due to the more competitive mobility of chains. Avrami exponent in this stage are between 3 and 4, indicating uniform nucleation and three dimension nucleation growth. The crystallization of EAA has transformed from nucleation control model at the beginning to overall growth model gradually. While at the secondary crystallization stage, EAA3003 > EAA3002 > EAA1410, which is mostly due to the effect of hydrogen bonding interaction. Mo's method investigated the crystallization behaviors of EAA in a different perspective. Three grades of EAA possess the following rate order: EAA3003 > EAA1410 > EAA3002. Difference from two approaches in relationship between the EAA1410 and EAA3002 are mostly owing to the higher amount of non-crystallizable chain ends. Both kinetics methods exhibit that EAA3003 crystallizes the fastest at the beginning of crystallization due to its low AA content.

The activation energy for non-isothermal crystallization of EAA3003, EAA3002, and EAA1410 were 326, 331, and 304 kJ mol⁻¹, respectively. It was proposed that the overall crystallization rate of EAA was affected by the interaction between the AA content, the chain mobility, and the quantity of non-crystallizable chain ends. Crystallization enthalpy ΔH_c declined with the increase of AA content, which reduced the number and length of ethylene chains. At the same cooling rate, the increase in AA content would lead to depression in the subsequent melting temperature and melting enthalpy ΔH_m .

References

- Luo N, Michael JS, Douglas EH. Surface modification of ethylene-co-acrylic acid copolymer films: addition of amide groups by covalently bonded amino acid intermediates. *J Appl Phys*. 2004;92(3):1688–94.
- Luo F, Zhang J, Wang XL, Chen JF, Xu ZZ. Formation of hydrophilic ethylene-acrylic acid copolymer microporous membranes via thermally induced phase separation. *Acta Polym Sin*. 2002;10(5):566–71.
- Zhang J, Luo F, Wang XL, Chen JF, Xu ZZ. The effect of kinetic factors on the structure of the hydrophilic ethylene-acrylic acid copolymer microporous membranes prepared via thermally induced phase separation. *Acta Polym Sin*. 2003;42(2):241–6.
- Kang N, Xu YZ, Wu JG, Feng W, Weng SF, Xu DF. The correlation between crystalline behavior of polyethylene segments and hydrogen bonds among carboxyl groups in ethylene-acrylic acid copolymers. *Phys Chem Chem Phys*. 2000;2(16):3627–30.
- Zhao HP, Lin WX, Yang GA, Chen Q. The structure and mobility of the noncrystalline region of ethylene-acrylic acid copolymers as studied by C-13 CP/MAS and VT H-1 wideline NMR spectroscopy. *Acta Polym Sin*. 2003;5:631–6.
- Xu WB, Liang GD, Wang W. Poly (propylene)-poly (propylene)-grafted maleic anhydride-organic montmorillonite (PP-PP-g-MAH-Org-MMT) nanocomposites. II. Nonisothermal crystallization kinetics. *J Appl Polym Sci*. 2003;88(14):3093–9.
- Nathaporn S, Nithitanakul M, Grady BP. Non-isothermal melt crystallization kinetics for ethylene-acrylic acid copolymers and ethylene-methyl acrylate-acrylic acid terpolymers. *Eur Polym J*. 2004;40(4):829–38.
- Brandrup J, Immergut EH. *Polymer handbook*. New York: Johnson Wiley & Sons Inc; 1999. p. v–17.
- Jeziorny A. Parameters characterizing the kinetics of the non-isothermal crystallization of poly(ethylene terephthalate) determined by d.s.c. *Polymer*. 1978;19(10):1142–4.
- Mya KY, Pramoda KP, He CB. Crystallization behavior of star-shaped poly(ethylene oxide) with cubic silsesquioxane (CSSQ) core. *Polymer*. 2006;47(14):5035–43.
- Joshi M, Butola BS. Studies on nonisothermal crystallization of HDPE-POSS nanocomposites. *Polymer*. 2004;45(14):4953–68.
- Avrami M. Kinetics of phase change (I): general theory. *J Chem Phys*. 1939;7(12):1103–12.
- Avrami M. Kinetics of phase change (II): transformation-time relations for random distribution of nuclei. *J Chem Phys*. 1940;8(2):212–24.
- Avrami M. Granulation, phase change and microstructure. *J Chem Phys*. 1941;9(2):177–84.
- Sanchez EMS. Ageing of PC/PBT blend: mechanical properties and recycling possibility. *Polym Test*. 2007;26(3):378–87.
- Yuan Q, Awate S, Misra RDK. Nonisothermal crystallization behavior of polypropylene-clay nanocomposites. *Eur Polym J*. 2006;42(9):1994–2003.
- An Y, Li L, Dong L. Nonisothermal crystallization and melting behavior of poly(β -hydroxybutyrate)-poly(vinyl-acetate) blends. *J Polym Sci B Polym Phys*. 1999;37(5):443–50.
- Zhang Q, Zhang Z, Zhang H, Mo Z. Isothermal and nonisothermal crystallization kinetics of nylon-46. *J Polym Sci B Polym Phys*. 2002;40(16):1784–93.
- Cai J, Han Y, Yuan Z. Crystallization behavior of syndiotactic and atactic 1, 2-polybutadiene blends. *Polym Int*. 2004;53(8):1127–37.
- Qian JS, He PS, Nie KM. Nonisothermal crystallization of PP/nano-SiO₂ composites. *J Appl Polym Sci*. 2004;91(2):1013–9.
- Ozawa T. Kinetics of non-isothermal crystallization. *Polymer*. 1971;12(3):150–8.
- Weng W, Chen G, Wu D. Crystallization kinetics and melting behaviors of nylon 6/foiated graphite nanocomposites. *Polymer*. 2003;44(26):8119–32.
- Li X, Guo W, Zhou Q, Xu S, Wu C. Non-isothermal crystallization kinetics of poly (ethylene terephthalate)/grafted carbon black composite. *Polym Bull*. 2007;59(5):685–97.
- Liu TX, Mo ZS, Wang S, Zhang HF. Nonisothermal melt and cold crystallization kinetics of poly(aryl ether ether ketone ketone). *Polym Eng Sci*. 1997;37(3):568–71.
- Liu M, Zhao Q, Wang Y, Zhang C, Mo Z, Cao S. Melting behaviors, isothermal and non-isothermal crystallization kinetics of nylon 1212. *Polymer*. 2003;44(8):2537–45.
- Ren M, Mo Z, Chen Q, Song J, Wang S, Zhang H, et al. Crystallization kinetics and morphology of nylon 1212. *Polymer*. 2004;45(10):3511–18.
- Song J, Chen Q, Ren M, Sun X, Zhang H, Zhang H, et al. Effect of partial melting on the crystallization kinetics of nylon-1212. *J Polym Sci B Polym Phys*. 2005;43(22):3222–30.
- Pisitsak P, Magaraphan R. Influences of a liquid crystalline polymer, vectra A950, on crystallization kinetics and thermal stability of poly(trimethylene terephthalate). *J Therm Anal Calorim*. 2009;95(2):661–6.
- Cebe P, Hong S-D. Crystallization behavior of poly (ether-etherketone). *Polymer*. 1986;27(8):1183–92.
- Augis JA, Bennet JD. Calculation of the Avrami parameters for heterogeneous solid state reactions using a modification of the Kissinger method. *J Therm Anal Calorim*. 1978;13(2):283–92.
- Kissinger HE. Variation of peak temperature with heating rate in differential thermal analysis. *J Res Natl Stds*. 1956;57(4):217–21.
- Păcurariu C, Lazău RI, Lazău I, Țița D. Kinetics of non-isothermal crystallization of some glass-ceramics based on basalt. *J Therm Anal Calorim*. 2007;88(3):647–52.
- Păcurariu C, Lazău RI, Lazău I, Stoleriu S. Kinetic study of the crystallization processes of some decorative ceramic glazes. *J Therm Anal Calorim*. 2007;88(3):641–5.
- Shi XM, Jin J, Chen SJ, Zhang J. *J Appl Polym Sci*. doi: 10.1002/app.